OXYGEN INDUCED REACTIONS AT 200 AND 60 GeV/NUCLEON*

WA80 COLLABORATION

H. R. SCHMIDT[1], R. ALBRECHT[1], T. C. AWES[2], C. BAKTASH[2], P. BECKMANN[3], G. CLAESSON[1], F. BERGER[3], R. BOCK[1], L. DRAGON[3], R. L. FERGUSON[2], A. FRANZ[4], S. GARPMAN[5], R. GLASOW[3], H. Å. GUSTAFSSON[5], H. H. GUTBROD[1], J. W. JOHNSON[2], K. H. KAMPERT[3], B. W. KOLB[1], P. KRISTIANSSON[4], I. Y. LEE[2], H. LÖHNER[3], I. LUND[1], F. E. OBENSHAIN[2], A. OSKARSSON[5], I. OTTERLUND[5], T. PEITZMANN[3], S. PERSSON[5], F. PLASIL[2], A. M. POSKANZER[4], M. PURSCHKE[3], H. G. RITTER[4], R. SANTO[3], T. SIEMIARCZUK[1], S. P. SORENSEN[2], E. STENLUND[5] AND G. R. YOUNG[2]

[1] Gesellschaft für Schwerionenforschung, Darmstadt, West Germany
[2] Oak Ridge National Laboratory, Oak Ridge, Tennessee, USA
[3] University of Münster, Münster, West Germany
[4] Lawrence Berkeley Laboratory, Berkeley, California, USA
[5] University of Lund, Lund, Sweden

(Received October 16, 1987)

The ultimate goal of ultra-relativistic heavy ion physics is the creation and detection of a new form of matter, the so-called Quark-Gluon Plasma (QGP). The QGP is a state of matter in which normal nuclear matter has been compressed to such an extent that the colour force field between the constituents of the nucleon is sufficiently screened that a deconfinement phase transition takes place. This paper presents a review of experimental possibilities of the WA80 experiment to detect signatures of the QGP phase and some first results.

PACS numbers: 25.70.Np

1. Introduction

The ultimate goal of ultra-relativistic heavy ion physics is the creation and detection of a new form of matter, the so-called Quark-Gluon Plasma (QGP). The QGP is a state of matter in which normal nuclear matter has been compressed to such an extent that the colour force field between the constituents of the nucleon is sufficiently screened that a deconfinement phase transition takes place [Sa86]. It is widely believed that the early universe, some 10^{-6} seconds after its creation, consisted of this form of primordial matter.

* Presented by H. R. Schmidt at the XXVII Cracow School of Theoretical Physics, Zakopane, Poland, June 3–15, 1987.

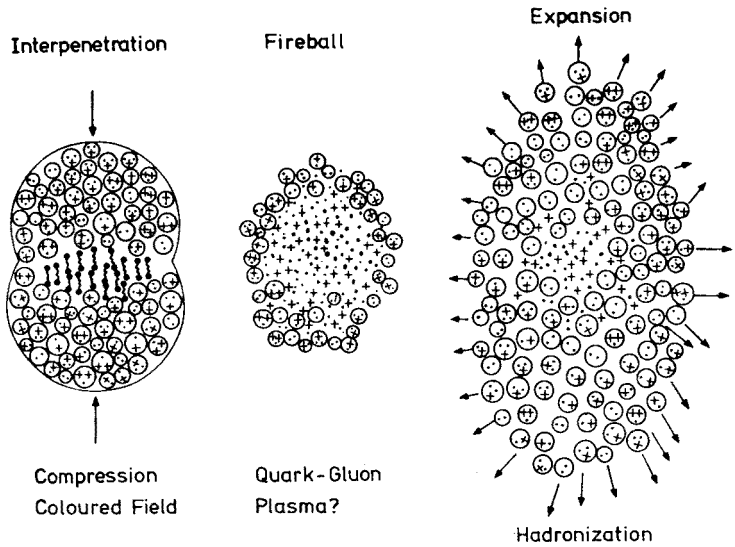

Fig. 1. Artists view of the space-time evolution of quark matter in an ultra-relativistic heavy-ion collision

Fig. 1 shows an artists view of the space-time evolution of quark matter, created in the laboratory by means of the ultra-relativistic collision of two heavy nuclei. If two nuclei of high energy collide, they will create a zone of hot and dense matter, eventually having an energy density high enough to "melt" the individual nucleons into a "soup" of freely moving quarks and gluons, the above described QGP. The QGP will rapidly expand, and quarks will hadronize, mainly into charged and neutral mesons. The (very difficult) experimental task is to search amongst and amidst the abundantly created mesons for signatures of the early QGP phase.

2. Experimental setup

In November 1987, ^{16}O beams of 200 and 60 GeV/nucleon, were delivered to five major experiments at the CERN SPS simultaneously. This opened for the first time the possibility to study ultra-relativistic heavy-ion collisions and to investigate the possible existence of a transition to the Quark-Gluon Plasma under controlled conditions in the laboratory. The setup of the WA80 experiment is shown in Fig. 2.

The experimental arrangement of WA80 [Al85] consists of the following detector systems: the Plastic Ball, several charged-particle multiplicity arrays, the MIRAC (Mid--Rapidity Calorimeter), SAPHIR (Single-Arm Photon Detector for Heavy-Ion Reactions), the time-of-flight wall, and the ZDC (Zero-Degree Calorimeter). In addition, the setup includes several beam counters, a thin (500 microns) aluminum spherical reaction chamber located inside the Plastic Ball, and 5-cm-diameter carbon-fiber/epoxy evacuated beam lines of 500-micron nominal thickness. Great care was taken to keep all extraneous material out of the reaction zone, resulting in negligible background levels during target-out operation. Thin targets were used to avoid significant contributions from secondary interactions.

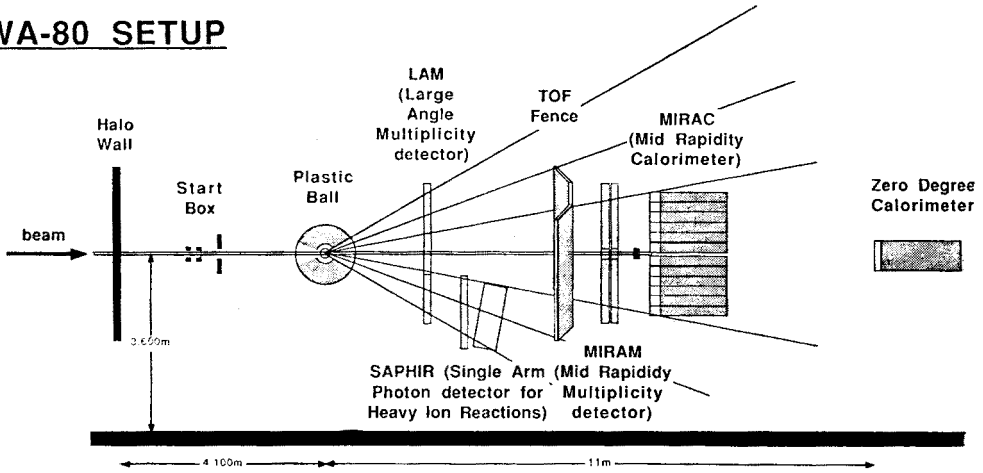

Fig. 2. Setup of the WA80 experiment

The target thicknesses were 185.7 mg/cm^2 of C, 200 mg/cm^2 of Cu and Ag, and 250 mg/cm^2 of Au. The beam level was limited to less than 2×10^6 particles/SPS spill. The detector systems of WA80 are described below in detail.

2.1. Plastic Ball

The Plastic Ball [BG82] is the only detector of WA80 that was in existence when the collaboration was formed. It had been in operation for five years at the LBL Bevalac, until it was moved to CERN in early 1986. It consists of 655 ΔE-E particle-identifying detectors, where the ΔE counters are CaF_2 crystals and the E counters are plastic scintillators. The two types of counters are optically coupled and read out by one photomultiplier. The signals are separated by pulse shape discrimination. The near 4π coverage of the Plastic Ball was decreased somewhat to avoid the shadowing of downstream detectors. The resulting pseudorapidity coverage is $-1.7 < \eta < 1.3$, correponding essentially to the rapidity region associated with target products. The device is operated in a mode in which it identifies and measures the energy of charged particles from protons through alphas, as well as positive pions.

The Plastic Ball serves the function of both a calorimeter and a multiplicity detector. It will provide results that can be viewed as extensions of the Plastic Ball Bevalac program. These include the study of matter flow from global analysis, determination of the extent of spectator drag from the measurement of the average value of p_{parallel} in the target rapidity region, estimates of entropy from measured d/p ratios, and the extraction of source sizes and timescales from particle-particle correlations.

2.2. Multiplicity arrays

A unique feature of WA80 is the essentially complete 4π coverage for the measurement of the multiplicity of charged particles (pseudorapidity range $-1.7 < \eta < 4.4$). Beyond the range of the Plastic Ball, this coverage is provided by a set of four charged-particle

multiplicity detectors, which are based on the Iarocci streamer tube technology. The tubes are made of carbon-coated plastic and filled with a mixture of isobutane and argon at atmospheric pressure. The central inner wire is kept at a potential of 4.8 kV. An impinging charged particle produces a local discharge (streamer) which is detected via capacitive coupling by means of a pad readout. The pads vary in size from 1×2.5 cm^2 to 4×5 cm^2 depending on their location. They are attached directly onto one side of a printed circuit board which also carries the readout electronics in the form of surface-mounted integrated circuits. The multiplicity arrays are

(*i*) Large-Angle Multiplicity Detector (LAM), located at 2.4 m from the target, covering the region between 30° and 10° and consisting of 5664 pads;

(*ii*) Mid-Rapidity Multiplicity Detector (MIRAM), located at 6 m, covering the region from 13° to 0.9° and consisting of a double layer of 8192 pads each;

(*iii*) Saphir Multiplicity Detector (SAM), located at 2.5 m, with $\Delta\theta = 10°$ and $\Delta\phi = 80°$ and consisting of 7200 pads. The two layers of MIRAM are located in front of the MIRAC, and SAM is located in front of SAPHIR.

Aside from generating charged-particle multiplicity data, the 29248-pad multiplicity arrays constitute an important component of the prompt trigger system by flagging events in which (*a*) at least N_{min} pads have fired (minimum bias) and (*b*) more than N_{high} pads have fired (high multiplicity events). In addition, MIRAM data are expected to enhance the information deduced from the MIRAC, and SAM measurements are needed to help identify charged-particle-induced hadronic showers in SAPHIR.

2.3. Mid-rapidity calorimeter

The ability to measure the transverse energy flux, $dE_t/d\eta$, in the mid-rapidity region is provided by the modular MIRAC. The design of the calorimeter is based on the uranium/plastic scintillator calorimeter of Akesson et al. [Ak85]. It consists of 30 stacks, and each stack contains six 20 cm by 20 cm towers, optically separated from each other by cuts in the plastic sampling material. Each tower consists of a lead-plastic electromagnetic section of 15 radiation lengths, providing an estimated containment of 97% for 1-GeV photons (91% for 30-GeV photons), and a steel-plastic hadronic section of 6.2 absorption lengths with an estimated longitudinal containment of 98% for 50-GeV protons. Each section is read out by dual wavelength-shifter plates located on the sides of the towers.

Extensive performance tests and calibrations of the MIRAC units have been carried out, at both the PS and the SPS accelerators. The resolution, linearity, containment, position response, and e/h response were evaluated. All of these quantities were found to be consistent with design expectations. At 10 GeV/c the e/p ratio was found to be 1.3, and the measured $\sigma/\sqrt{E}$ resolutions were 46% for charged pions and 17% for electrons. The final calibration of all calorimeter towers was made in the X1 beam line of the SPS with 10-GeV/c electrons, muons, and pions. The photomultiplier response to a laser pulser, from which light is injected into the front of each wavelength-shifter plate, was also determined at that time. This procedure made it possible to recover the calibration after the calorimeters were installed in their final location in the H3 beam line.

Twenty-four of the MIRAC stacks are deployed symmetrically around the beam

line at 6.5 m, covering a pseudorapidity range $2.4 < \eta < 5.5$. Taking into account the Plastic Ball, WA80 lacks the detectors necessary for the measurement of the total transverse energy flux only in a region that is slightly larger than one unit of pseudorapidity, i.e., from $1.3 < \eta < 2.4$. The remaining six stacks of the MIRAC, however, are located in this pseudorapidity gap adjacent to the bulk of the calorimeter, and, together with LAM and with the original time-of-flight wall of the GSI-LBL Plastic Ball collaboration, they constitute a unique single-arm detector that is capable of sampling the Z-distribution in this region and is also expected to yield information on the distribution of neutrons and of antibaryons.

The MIRAC towers covering the forward mid-rapidity region are used to generate a prompt trigger signal, flagging events with high-E_t values. This is accomplished by means of weighted linear summing of dynode signals.

2.4. SAPHIR

The SAPHIR detector consists of 1278 active lead-glass modules, each of dimensions $3.5 \times 3.5 \times 46$ cm^3, arranged to cover an area of 98.0×171.5 cm^2. The center of the front surface of the detector is located at 3.12 m from the target and at 20° with respect to the beam direction, covering an approximate pseudorapidity range of $1.5 < \eta < 2.1$. The choice of module size is based primarily on the results of the GAMS [Bi81] collaboration, and the 18 radiation lengths of SF5 lead glass guarantee a 98% shower containment for 30-GeV photons.

Prototype detector tests have been carried out at DESY with electrons of 0.6 to 6 GeV, and extensive further tests and calibrations have been carried out at the CERN PS and SPS accelerators. The results were found to be either consistent with, or somewhat superior to, design expectations. The energy resolution $\sigma/\sqrt{E}$ was found to be $(6.0/\sqrt{E}+0.4\%)$, corresponding to a $\pi^0(\eta^0)$ mass resolution of a few percent, dependent on the $\pi^0(\eta^0)$ energy. The position resolution is better than 4 mm, and adjacent shower separation is possible for distances greater than 2.4 cm at the surface of the detector. The π^0 reconstruction efficiency rises from 20–30% at low (0.2–0.3 GeV/c) values of the pion transverse momentum, p_t, to about 80% at 2 GeV/c and about 90% at 6 GeV/c. At still larger values of p_t, the π^0 efficiency decreases. A sharp π^0 peak was obtained in the invariant mass spectrum, reconstructed on-line, for events with $E_{\gamma\gamma}$ greater than 2.5 GeV, and distinct π^0 peaks were also obtained at lower $E_{\gamma\gamma}$ energies. SAPHIR is another component of the prompt trigger system, flagging events with a minimum number of high-energy photons. As in the case of the Plastic Ball and the MIRAC, its calibration and stability are determined by means of a laser pulser.

2.5. Zero degree calorimeter

The final WA80 detector to be discussed is the Zero-Degree Calorimeter (ZDC). This 8-ton uranium-plastic sampling calorimeter is located behind the 7.5 cm by 7.5 cm beam line hole in the MIRAC and is a key component of the trigger system. The three primary design considerations were near-total containment for protons of 225 GeV, excellent energy resolution, and fast count-rate capability. A design criterion, based on

simulation calculations, was the ability of the ZDC to distinguish between the simultaneous incidence of either 15 or 16 nucleons of 50 GeV. The dimensions of the ZDC are 60 cm × 60 cm × 189 cm, with an electromagnetic section of 17 cm and a hadronic section of 172 cm.

3. Event characterization and trigger

Fig. 3 shows a more schematic view of the setup. It serves to illustrate how interesting events are selected and characterized. Since a high energy density is the necessary prerequisite for the creation of the QGP, primarily events promising this should be enriched by the online trigger selection.

A beam particle of energy E transfers an amount ΔE to the target. The remaining energy $E-\Delta E$ is measured by the ZDC. Thus by triggering on low energies in the ZDC one ensures a high energy transfer to the target nucleus. A subset of these events has a component of high transverse energy. Since the transferred energy ΔE, except for some relatively small losses at angles beyond 11°, is measured in the MIRAC, these events are detected, and a trigger of high priority is set. Furthermore events with low energy in the ZDC might be associated with a large number of secondaries. Again a trigger of high priority is set if such an event is detected in the $\approx 4\pi$ multiplicity array. Thus an interesting event is characterized (online) by little energy in the ZDC, and/or a large transverse energy flux and/or high multiplicity of secondaries.

The "Minimum Bias" trigger, on the other hand, requires that:

(*i*) the energy detected in the ZDC be less than 90% of the projectile energy;

(*ii*) that at least one charged particle be detected with $\eta < 4.4$.

The experimental "proof" that almost all the energy of the event is contained in the $\approx 2\pi$ calorimeter coverage is shown in Fig. 4. The energy measured in the ZDC in the angu-

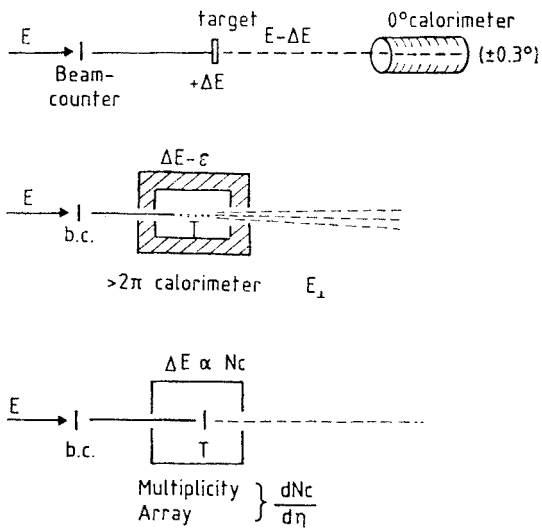

Fig. 3. Schematic view of the WA80 setup

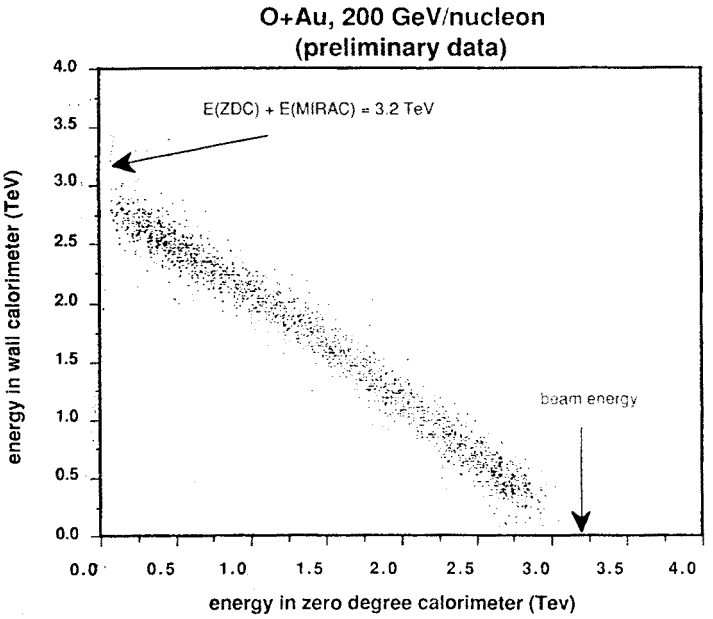

Fig 4. Event-by-event plot of the energy measured in the mid-rapidity calorimeter versus the energy measured in the zero degree calorimeter

lar range from 0°–0.3° is plotted versus the energy in MIRAC for the reaction 3.2 TeV $^{16}O+^{197}Au$. Except for the lower ZDC energies, where some energy escapes beyond angles of 11.3°, all events lie on the line of constant, full energy.

4. Transverse energy spectra and energy densities

One very important aspect of nucleus-nucleus collisions is the effect of the nuclear geometry on the experimental results. This is clearly illustrated in Fig. 5, in which the ZDC energy spectra are shown. It can be seen that, in the case of $^{16}O+C$ at 200 GeV/nucleon, the cross section is practically zero for energies below 800 GeV, indicating that, for every event, at least four projectile nucleons enter the ZDC with full beam energy. As the target size increases, this picture changes progressively, until at the lowest energies, a peak is observed in the case of $^{16}O+Au$. This originates from the fact that, for heavier targets, a much wider range of impact parameters gives rise to collisions in which the entire projectile interacts with a nearly constant number of target participants. This number is sufficiently large that there is an absence of projectile spectators in the beam direction. In Fig. 5 the experimental data (open circles) are compared to a model calculation in which the nucleus-nucleus version (FRITIOF) of the Lund model [NS87] was used. As can be seen the model predictions describe the experimental data well.

The transverse energy (E_t) spectra are presented in Fig. 6, and once again the importance of the geometry of the colliding nuclei can be pointed out. This is demonstrated in the case of ^{16}O + Au by the peak at high transverse energy. This peak is closely related

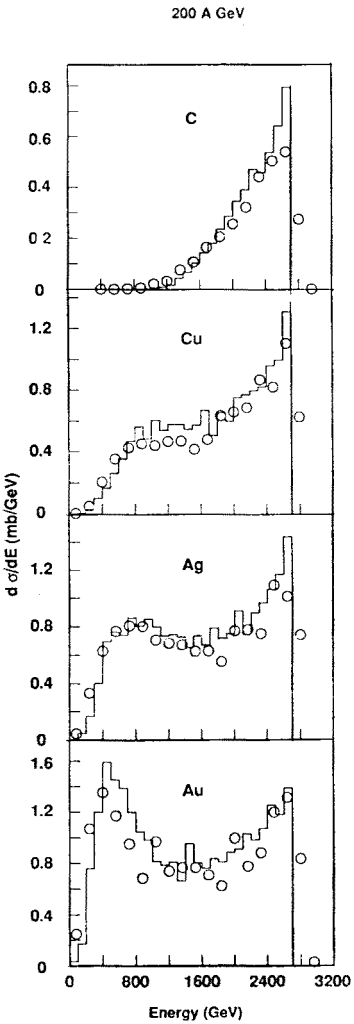

Fig. 5

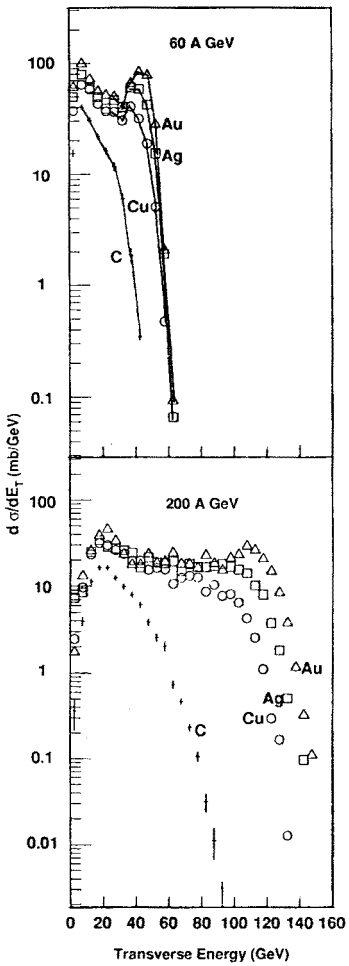

Fig. 6

Fig. 5. ZDC energy spectra for the reactions ^{16}O + C, Cu, Ag, Au at 200 GeV/nucleon. The histograms are the predictions from the FRITIOF model (see text)

Fig. 6. Transverse energy distributions for the reactions ^{16}O+C, Cu, Ag, and Au at 60 and 200 GeV/nucleon

to the peak in the low energy region of the ZDC spectrum shown in Fig. 6. One striking feature of Fig. 6 is that at 60 GeV/nucleon the tails of the energy spectra for the different targets almost coincide with each other. At first glance, this appears to indicate a saturation of the produced transverse energies, as might be expected if complete nuclear stopping were observed in all cases. However, at this bombarding energy, this effect is more likely to be due to a combination of two effects which tend to cancel each other. One effect is that of increasing transverse energy with increasing target mass, and the other is the decreasing pseudorapidity of the effective center of mass, which leads to a decreased coverage by

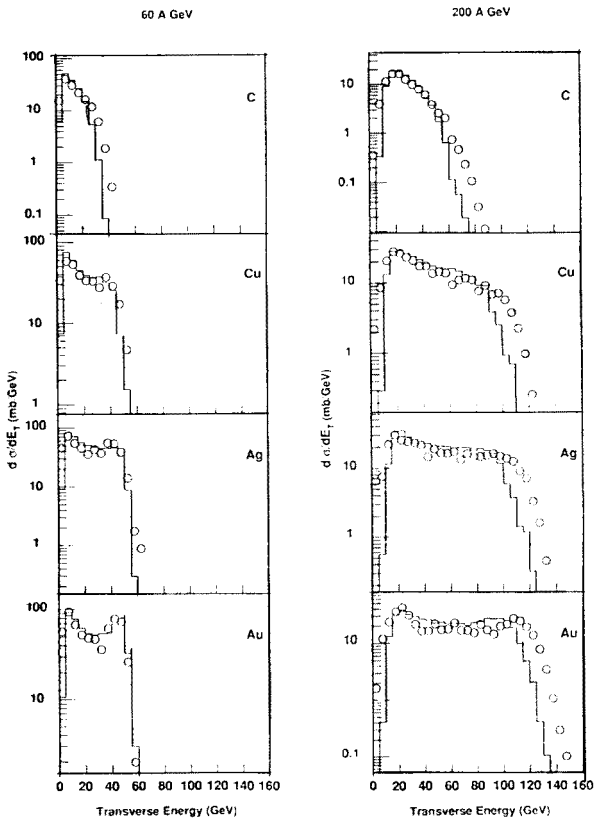

Fig. 7. Experimental transverse energy distributions (open circles) compared to FRITIOF model calculations (histograms) for the reactions ^{16}O + C, Cu, Ag, and Au at 60 and 200 GeV/nucleon

MIRAC. A similar effect can also be seen for the 200 GeV/nucleon data, but in this case the transverse energy grows faster than the reduction in coverage and leads to a net increase of the transverse energy in the region of the tails. Fig. 7 shows the experimental transverse energy distribution (open circles) compared to the FRITIOF calculations (histograms) for the different targets at 60 and 200 GeV/nucleon. As can be seen, the model calculations fit the data very well for all four targets at 60 GeV/nucleon, while they somewhat underpredict the experimental data at 200 GeV/nucleon.

The degree of nuclear stopping and the attained energy densities are two of the key quantities that relate to the probability of QGP formation. Estimates of these quantities based on our data are presented here. Transverse energies of fully stopped systems, E_t^{max}, can be estimated and compared with measured E_t values under the assumption that: in central collisions all the projectile nucleons react with a cylinder of the target nucleus which has a base area equal to the cross section of the projectile; and that all of the available center of mass energy, subtracting the mass of the participating baryons, is emitted isotropically in the CM system. The results, considering only central events, are given in Table I. It can be seen from the table that nuclear stopping decreases from about 90% at 60 GeV/nucleon

TABLE I

	60 GeV/nucleon	200 GeV/nucleon
E_{cm}	320	580
E_t^{max}	200	400
E_t^{max} (MIRAC)	62	200
E_t^{obs} (MIRAC)	55	120
stopping	90%	60%

to about 60% at 200 GeV/nucleon. Corresponding estimates of the range of energy densities [Bj83] reached are 0.5 to 1.0 GeV/fm^3 at 60 GeV/nucleon and 1.0 to 2.6 GeV/fm^3 at 200 GeV/nucleon, with tails of the event distribution reaching as high as 3 GeV/fm^3 in the higher energy case. These energy densities are believed to be close to those required for the formation of the quark-gluon plasma.

5. *Multiplicities*

We focus here on studies of impact-parameter, target-size, and projectile-energy dependence of charged particle production. Charged particle multiplicity and pseudorapidity distributions are presented for the pseudorapidity range $-1.7 < \eta < 4.2$ for oxygen collisions with nuclei of various targets. The measured distributions are compared to the Lund model (FRITIOF) and to HIJET [Lu85].

The data were obtained under the minimum bias condition. Corrections were made for multiple hits. The correction is typically of a few percent except in the forward-most region and for the most violent collisions, where it can reach up to 20%. The efficiencies of the detectors are estimated by correlating hits in overlapping portions. The overall

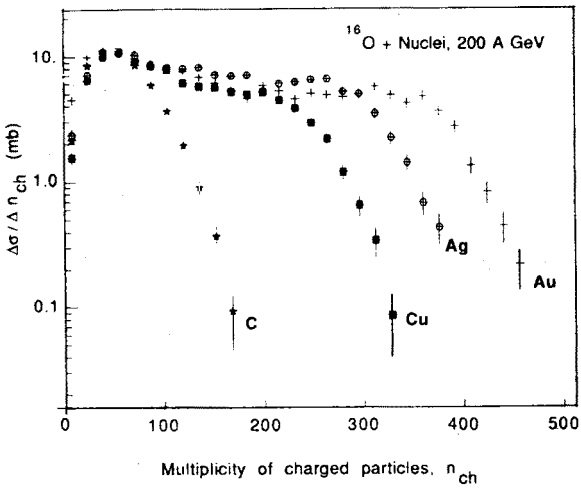

Fig. 8. Charged particle multiplicities measured for $-1.7 < \eta < 4.2$ for 200 GeV/nucleon ^{16}O + C, Cu, Ag, and Au

efficiency of each detector plane was found to be 85%. Contributions from secondary interactions, from converted photons, and from decays of strange particles, such as K_0^{short} and Λ's, are included in the present data sample. Depending on the kinematic region, it is estimated that these processes, together, contribute typically 5–10% to the charged particle yield.

The trigger conditions were simulated in all model calculations. In Fig. 8, charged particle multiplicities are presented for 200 GeV/nucleon oxygen collisions with target nuclei of carbon, copper, silver and gold. It can be seen that events with multiplicities up to 500 are observed. Subtracting baryons from target fragmentation, this corresponds to the production of about 400 charged particles. More detailed information on the reaction mechanism is contained in the pseudorapidity distributions. These are presented in Fig. 9 for 200 GeV/nucleon ^{16}O incident on the four targets C, Cu, Ag and Au, together with FRITIOF and HIJET model calculations. The calculations significantly underestimate the data at mid-rapidities ($\eta \approx 3.0$), as well as in the target rapidity region. The excess at target rapidities is most likely due to the non-inclusion of target fragmentation processes in the model calculations.

Fig. 10 shows for the reaction ^{16}O + Au at 200 GeV/nucleon, the charged particle multiplicity density in the mid rapidity region plotted versus the energy measured in the ZDC. The width of the distribution indicates a larger variation in the dynamics of the collision as predicted by the FRITIOF calculations.

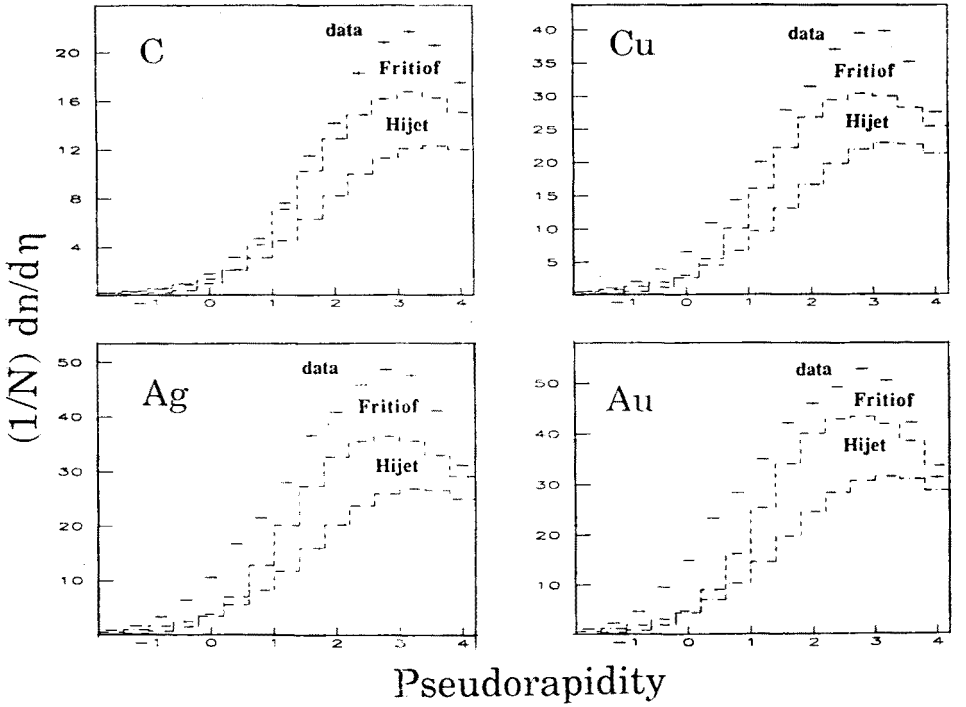

Fig. 9. Pseudorapidity distributions, $dN_c/d\eta$, for 200 GeV/nucleon ^{16}O + C, Cu, Ag, and Au, compared to model results from FRITIOF and HIJET

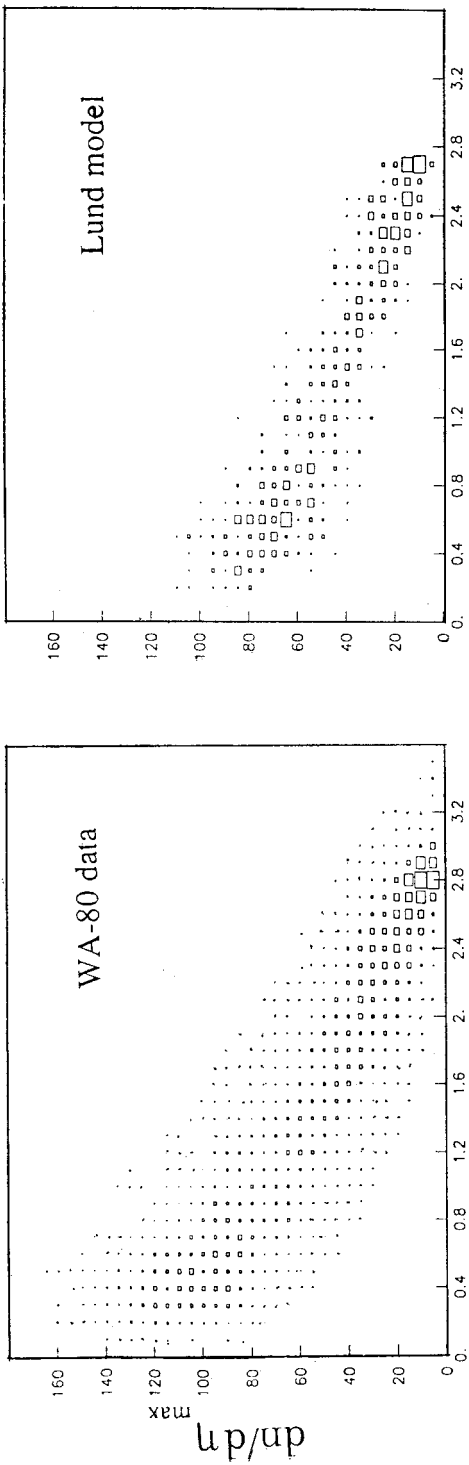

Fig. 10. Charged particle density in mid-rapidity vs energy at zero degrees as measured event by event for 200 GeV/nucleon ^{16}O + Au.

A comparison with the theoretical models is more appropriate in these data, since, e.g., the target rapidity can be ignored where the models do not claim to have a proper treatment of secondary reactions inside the nucleus. In addition the potential problem of simulating the trigger in the model calculation is absent when the distributions are compared in the region of little remaining energy at zero degree.

Summarizing, charged particle distributions have been measured as a function of target mass and impact parameter. Deviations from the FRITIOF and the Hijet models are observed and are strongest for the Au data.

6. Photon spectra

The SAPHIR detector has been designed to investigate one of the promising signatures of the formation of QGP, the production of direct photons. In order to be able to determine the spectrum of direct photons, the detector has to be able to handle the large background of photons from the decay of neutral pions and eta mesons. This can only be achieved by the reconstruction of the decaying-meson events, and the high-granularity SAPHIR is, therefore, also an excellent detector for the measurement of neutral pion spectra. An example of the reconstruction of π^0's is shown in Fig. 11. Plotted are the invariant mass spectra, $M_{\gamma\gamma}$, for the cases $^{16}O + C$ and $^{16}O + Au$, showing that, even in the high multiplicity environment of $^{16}O + Au$, the π^0 peak can be well distinguished from the combinatorial background.

Inclusive photon spectra have been accumulated under the following conditions:

(*i*) No charged particle hit is observed in either one of the two layers of streamer tubes (charged particle veto).

(*ii*) The transverse shower development is compatible with that of an electromagnetic (EM) model shower of the same energy at the same point of incidence (χ^2 minimisation procedure).

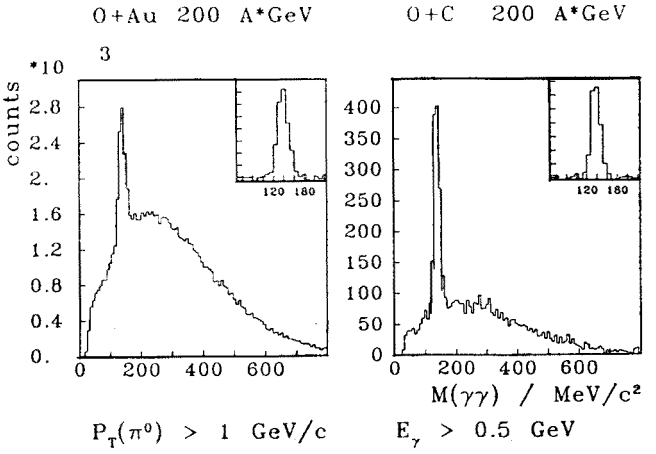

Fig. 11. Invariant mass spectra of $\gamma\gamma$-pairs for $^{16}O+Au$ and $^{16}O + C$ at 200 A GeV

Fig. 12 shows an example of an inclusive photon p_t spectrum accumulated under minimum bias trigger conditions and selected for low energy in ZDC (<10% of beam energy), which corresponds to a central collision selection. The slope of the photon p_t distribution for ^{16}O + Au deviates significantly from the slope of FRITIOF model results for equivalent conditions. The slope parameter T_{eff} for an exponential parametrization is about twice as large at $p_t > 0.4$ GeV/c as at $p_t < 0.4$ GeV/c. The FRITIOF model results can be well described by a $T_{eff} \approx 160$ MeV for all multiplicities and for O + nucleus as well as p + nucleus reactions. In order to analyze the high p_t tails of the inclusive photon spectra with respect to their mass and centrality dependence, we investigated the following procedures:

(*i*) fitting an exponential to the dN/dp_t distributions for $p_t > 400$ MeV/c.

(*ii*) calculating the average p_t from the truncated p_t distributions [Be85] by integrating the experimental data, where a lower cutoff was chosen at 400 MeV/c.

Both methods give qualitatively the same results. An example using method (*ii*) is shown in Fig. 13. Here an increase of 15% in the $\langle p_t \rangle_\gamma$ cut is observed for 200 GeV/nucleon ^{16}O + Au as a function of the centrality measured by the energy in ZDC. For the lighter systems and lower incident energy the increase is less pronounced. The FRITIOF model predicts almost no variation with centrality or target mass, however tends to describe the experiment for peripheral reactions. The increase in $\langle p_t \rangle_\gamma$ is even more pronounced if method (*i*) is applied; however, the fitting procedure introduces some uncertainty, while method (*ii*) gives uniquely defined values. The deviation from FRITIOF is obvious, although it has to be noted that in this model hard scattering is not included, which may account for at least part of the observed effect. Further investigations, especially after relating the energy in ZDC to the multiplicity density per participating baryon, may give sensitive results for

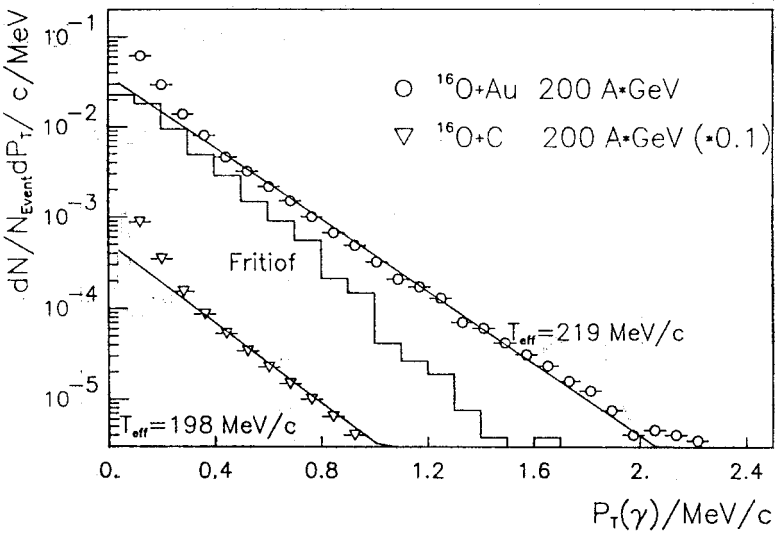

Fig. 12. Inclusive photon p_t spectrum accumulated under minimum bias trigger condition and selected for low energy in ZDC. For comparison with exponential parametrizations (solid lines) the FRITIOF model results are included as a dashed line

comparisons to models assuming pion radiation or hydrodynamic expansion [Ka86], [Bl87], [Da83].

In Fig. 14 the invariant cross sections for well identified π^0's are shown as a function of p_t for different target mass and energies and minimum bias trigger condition. The slope of these spectra for $p_t > 1$ GeV/c can be well described by exponentials whose inverse slope parameter gradually increases with target mass from $T_0 = 190$ MeV/c for carbon to $T_0 = 215$ MeV/c for the Au target at 200 A GeV. This behavior is consistent with the

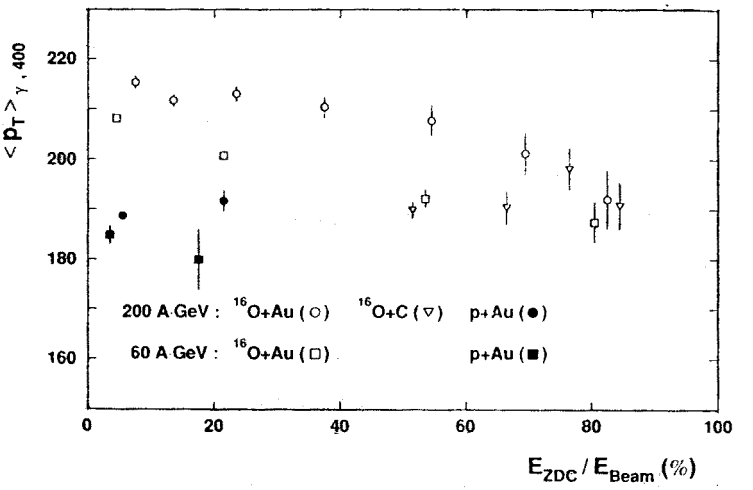

Fig. 13. Experimental $\langle p_t \rangle_\gamma$ cut for photons from the truncated distribution (see text) as function of centrality of the reaction defined by the energy deposited in ZDC, in percent of beam energy

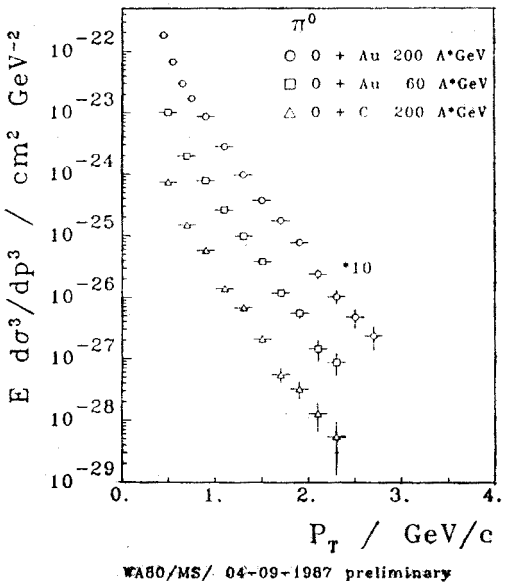

Fig. 14. Invariant cross sections for π^0 as function of p_t for different target mass and oxygen beam energies

observations from above; however, the statistical accuracy of the pion spectra from a limited amount of analyzed data ($\approx 10\%$ at present) is still too poor to perform any further selections according to the centrality of the reaction. A striking feature of the spectra in Fig. 14 is the change in slope at around $p_t = 1$ GeV/c, which is most pronounced for the heavy system and could have been deduced already from the inclusive photon data. This effect is not seen in proton proton reactions at 250 GeV/c incident momentum [Ha87] but is consistent with alpha alpha reactions at the ISR [An87].

Summarizing, we have presented inclusive photon spectra and p_t distributions for well identified π^0's from 200 and 60 GeV/nucleon ^{16}O + nucleus reactions. The π^0 mass resolution is sufficient to detect the π^0 signal in the invariant mass distribution of $\gamma\gamma$-pairs with good accuracy, even in the high multiplicity environment of ^{16}O + Au reactions. Inclusive photon spectra show a target mass and centrality dependence in the region $p_t > 500$ MeV/c not predicted in the current Fritiof model, which, however, does not take hard scattering into account. The π^0-p_t distributions taken under minimum bias trigger conditions confirm the target mass dependence. They display a change in slope at $p_t \approx 500$ MeV/c which is not seen in proton proton experimental data at comparable energy and not predicted in the FRITIOF model.

7. *Target fragmentation*

The target fragmentation region is covered by the Plastic Ball spectrometer. Fig. 15 shows the distribution of target *and* projectile baryons under minimum bias conditions. The shaded area represents the baryon distribution measured with the Plastic Ball. It includes particles up to ^4He and is corrected for the non-observed free neutrons. The lower curve is the result of a LUND model calculation yielding the *participating* target and projectile baryons. Two "bumps" at $\eta \approx 1.9$ and $\eta \approx 5.3$, corresponding to target and projectile participants, respectively, are clearly seen. It is of interest how many of the

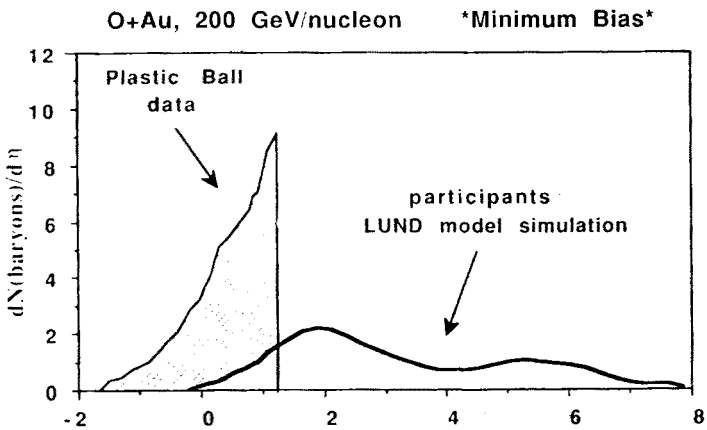

Fig. 15. Pseudorapidity distributions of target and projectile baryons. The shaded area represents the baryon distribution measured with the Plastic Ball. The solid curve is the result of a LUND model calculation yielding the participating target and projectile baryons. The y-axis units are arbitrary

total number of baryons in the system were measured in the Plastic Ball. Fig. 16 gives the average number of baryons per event in the Plastic Ball as a function of the energy in the zero degree calorimeter, hence, of increasing centrality of the collisions as the ZDC energy decreases. As can be seen, e.g. for the case ^{16}O + Au, the average number of baryons in the target region is about 124+/−10% for the most central collision. The uncertainty of +/− 10% is a systematic error due to the lack of particle identification in the region where protons punch through and overlap with pions. The Lund model, on the other hand, yields about 75 participating baryons. Combining the two figures, we can conclude that, for the most central collision enough energy is transferred to the target nucleus to allow complete disintegration into particles with $Z < 3$. With decreasing centrality of the collisions, more and more low energy heavy fragments are produced. These particles were not detected in the Plastic Ball, resulting in the observed decrease of the number of baryons

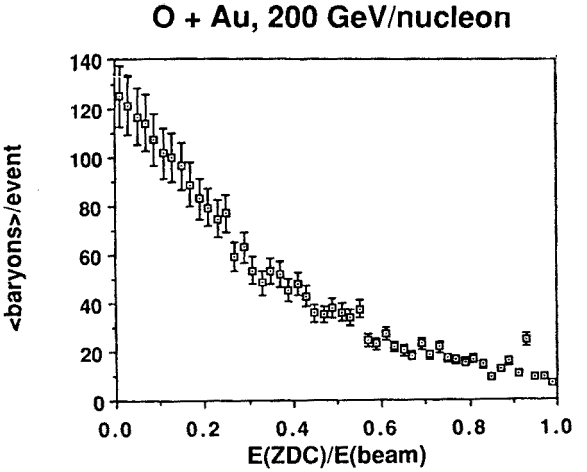

Fig. 16. Average number of baryons in the Plastic Ball for the reaction ^{16}O + Au at 200 GeV/nucleon as a function of the energy in the zero degree calorimeter

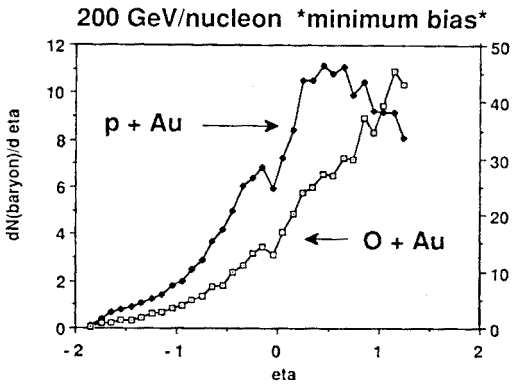

Fig. 17. Comparison of the η-distributions of baryons emitted from heavy-ion- and proton induced reactions at 200 GeV/nucleon

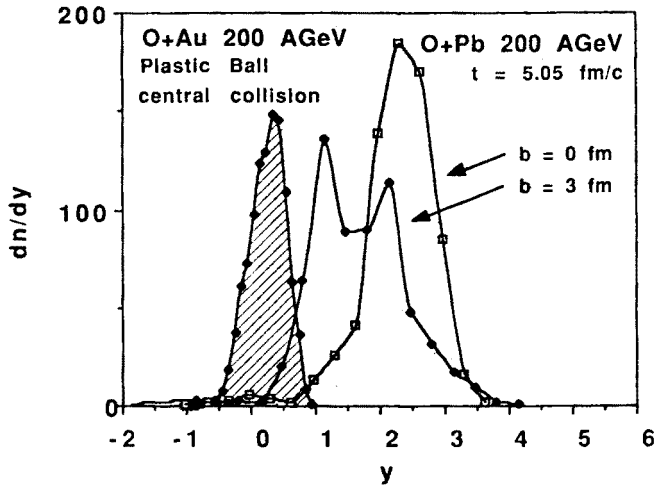

Fig. 18. Comparison of the experimental rapidity distribution of target baryons (shaded area) with a prediction from a one-fluid hydrodynamical model (see text)

with ZDC energy. The presence of these low energy heavy fragments, however, was clearly seen by the NA37 experiment [Bl87].

Fig. 17 compares the η-distribution of baryons emitted from heavy-ion and proton induced reactions at 200 GeV/nucleon. The two distributions clearly differ: The η-distribution from p + Au peaks inside the range of the Plastic Ball, while the baryons from ^{16}O-induced reactions are much more accelerated into the forward direction. The average shifts in rapidity $\langle \Delta y \rangle$ are 0.15 and 0.3 units of rapidity for proton and ^{16}O-induced reactions, respectively. Fig. 18 compares the experimental rapidity distribution of target baryons with a prediction within a one-fluid hydrodynamical model [Re87]. The theoretical distributions are calculated for impact parameters $b = 0$ and $b = 3$ fm, respectively. The experimental distribution is for central collisions, sampling impact parameters of $b = 0$ to about 4 fm. Considering the fact that the experimental distribution represents about 65% of all baryons of the system ^{16}O + Au, it becomes evident that the simplified description of the reaction with a one-fluid hydrodynamical model produces too much "drag" of the target fragments towards mid-rapidity.

REFERENCES

[Ak85] T. Akesson et al., *Nucl. Instrum. Methods* **A241**, 17 (1985).
[Al86] R. Albrecht et al., Report No. GSI-85-32, Gesellschaft für Schwerionenforschung, D-6100 Darmstadt, West Germany, 1985.
[An87] A. L. S. Angelis et al., *Phys. Lett.* **B185**, 213 (1987).
[Ba82] A. Baden et al., *Nucl. Instrum. Methods* **203**, 189 (1982).
[Be85] W. Bell et al., *Z. Phys.* **C27**, 191 (1985).
[Be87] B. Berthier et al., *Phys. Lett.* **B193**, 417 (1987).
[Bi81] F. Binon et al., *Nucl. Instrum. Methods* **188**, 507 (1981).
[Bj83] J. D. Bjorken, *Phys. Rev.* **D27**, 140 (1983).

[B187] J.-P. Blaizot et al., *Phys. Lett.* **B191**, 21 (1987).
[Da87] M. Danos et al., *Phys. Rev.* **D27**, 67 (1983).
[Ha87] P. van Hal, thesis: Particle Production in Hadron-Proton Interactions at 250 GeV/*c* Incident Beam Momentum, CERN 1987.
[Ka86] M. Kataja et al., *Phys. Rev.* **D34**, 2755 (1986).
[Lu85] T. W. Ludlam, BNL Report 51921, 3, 73 (1985).
[NS87] B. Nilsson-Almqvist et al., *Com. Phys. Comm.* **43**, 387 (1987).
[Re87] T. Rentzsch et al., *Mod. Phys. Lett.* **A2**, 193 (1987).
[Sa86] H. Satz, *Nature* **324**, 116 (1986).